RSC Advances

ROYAL SOCIETY OF CHEMISTRY

www.rsc.org/advances

TOC

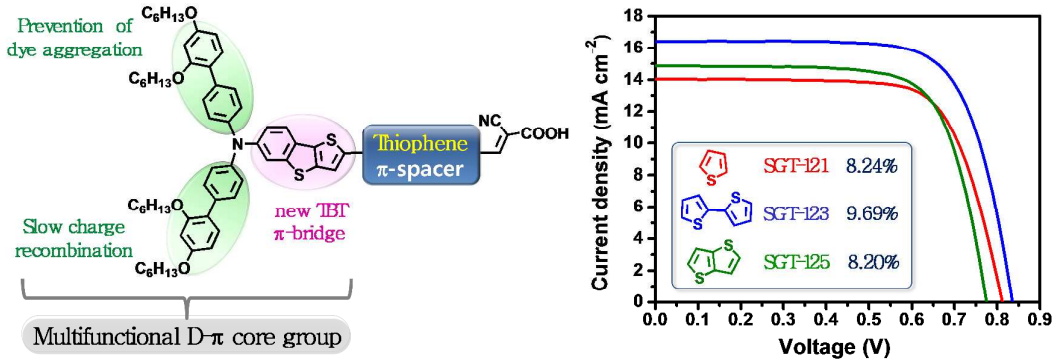

Table of Contents

D-π-A stuructured thieno[3,2-*b*][1]benzothiophene-based organic sensitizers with π-extended thiophene spacers are designed and synthesized for dye-sensitized solar cells. By investigating the structure-property relationships, the sensitizer containing bithiophene π-spacer exhibited the best performance (9.69%) with a cobalt electrolyte.

New Thieno[3,2-*b*][1]benzothiophene-Based Organic Sensitizers Containing π-Extended Thiophene Spacers for Efficient Dye-Sensitized Solar Cells

Yu Kyung Eom[a], Sung Ho Kang[a], In Taek Choi[a], Eunji Kim [b], Jeongho Kim[b], Myung Jong Ju[a] and Hwan Kyu Kim[a,*]

[a]*Global GET-Future Lab. & Department of Advanced Materials Chemistry, Korea University, 2511 Sejong-ro, Sejong 339-700, Korea, E-mail: hkk777@korea.ac.kr*

[b]*Department of Chemistry, Inha University, 100 Inha-ro, Incheon 402-751, Korea*

Electronic supplementary information (ESI) available. See DOI:

Abstract

Three new thieno[3,2-*b*][1]benzothiophene (**TBT**)-based D–π–A organic sensitizers containing the thiophene π-spacer (**SGT-121**, **123** and **125**) have been synthesized for the application of dye-sensitized solar cell (DSSC), where **TBT** was employed as a new fused π-bridge unit using the advantages of good co-planarity with the linkage between the thiophene unit and the phenyl unit of the triphenylamine group. Specifically, the combination of a dihexyloxyphenyl-substituted biphenylamine donor and the **TBT** π-bridge plays multifunctional roles, e.g., the enhanced ability of the π-bridge and donor, slow charge recombination and prevention of dye aggregation in the D–π–A sensitizer. The photophysical, electrochemical and photovoltaic properties of the **SGT** sensitizers were systematically investigated. As a strategy for the improvement of absorption abilities, the various thiophene derivatives, e.g., those with thiophene (**T, SGT-121**), bithiophene (**BT, SGT-123**) and thienothio[3,2-*b*]thiophene (**TT, SGT-125**) moieties, were incorporated as π-spacers between the **TBT** π-bridge and the acceptor unit. The introduction of thiophene π-spacers significantly improved the photovoltaic performance (in particular, in terms of the photocurrent J_{sc} and open-circuit voltage V_{oc}) compared to **SGT-127** without the thiophene unit. The **SGT** sensitizers were systematically evaluated for DSSCs based on the $Co(bpy)_3^{2+/3+}$ (bpy=2,2'-bipyridine) redox couple. Among the four **SGT** sensitizers, **SGT-123**-based DSSC including the **BT** moiety exhibited the highest power conversion efficiency of 9.69%, J_{sc} of 16.16 mA cm^{-2}, V_{oc} of 830 mV and fill factor of 0.72. These results present the impact of thiophene π-spacers for enhancing the photovoltaic performances of D–π–A organic sensitizer.

Introduction

The current shale-gas revolution brings about a new phase of low oil prices, but the global energy experts anticipate being faced with an energy crisis in the near future. As one of the alternate energy technologies, dye-sensitized solar cells (DSSCs) have received continuous attention, owing to their low fabrication cost, transparency, full colour and flexibility with respect to silicon-based solar cells.[1,2] The components of DSSCs, such as sensitizers, redox electrolyte and semiconductor metal oxide, have been investigated in order to achieve a high power conversion efficiency (PCE).[3,4] With the diverse sensitizers as the important component in enhancing the PCE, ruthenium (Ru)-complex-based DSSCs have achieved a PCE over 11%,[5] whereas the zinc (Zn) porphyrin sensitizer (SM315)-based DSSC has shown a PCE over 13%.[6] In contrast with the Ru-complex, metal-free organic sensitizers have become attractive sensitizers, owing to their high molar extinction coefficients,[7] facile engineering of their optical properties,[8,9,10] low cost and relatively high PCEs over 10%.[11] Most of the reported, efficient, metal-free organic sensitizers are commonly composed of the donor–π-bridge–acceptor (D–π–A) configuration, which exhibits efficient intramolecular charge-transfer (ICT) properties for favourable electron injection from the excited dye to the conduction band of TiO_2 (E_{CB}).[12,13]

For new breakthroughs in achieving higher PCEs, the development of the π-bridge unit is fundamental in the molecular engineering of D–π–A sensitizers, which should be introduced as planar-type building blocks of fused heterocycles instead of twisted structures.[4,13,14] The various fused heterocycles such as thienothiophene,[15] dithienothiophene (**DTT**),[16] dithieno[3,2-*b*:2',3']silole (**DTS**),[17] 4*H*-cyclopenta[2,1-*b*:3,4-*b*']dithiophene (**CPDT**),[8,18,19] dithieno[3,2-*b*:2',3']pyrrole (**DTP**),[20] benzo[1,2-*b*:4,5-*b*']dithiophene (**BDT1**)[21] and benzo[2,1-*b*:3,4-*b*']dithiophene (**BDT2**)[22] have been incorporated into the π-bridges with broad and

intense spectral absorption in the visible-light region. Among these fused heterocycles, the **CPDT** π-bridge exhibited a record PCE over 10%,[8,11,23] which has many advantages such as a rigid co-planar structure, good electron-donating ability, enhancement of the photocurrent for efficient charge transfer[24] and prevention of dye aggregation by the long alkyl chain.[25]

By merging insights from the good co-planar structure with the reduction in dihedral angle between the thiophene unit and the phenyl unit of the triphenylamine (**TPA**) donor,[26] we developed thieno[3,2-*b*][1]benzothiophene (**TBT**) as the new fused π-bridge for highly efficient metal-free organic sensitizers.[27] The **TBT** derivatives have also been widely employed as core materials for ferroelectric liquid crystals (**FLC**)[28] and organic thin-film transistors (**OTFT**)[29] with good electrical performances, strong fluorescence and high ambient stabilities.[30] For optimal D–π–A sensitizers, the dihexyloxyphenyl-substituted biphenylamine donor and **TBT** π-bridge unit (compound **1** in **Scheme 1**) were combined as a multifunctional core group, which could play various roles for enhanced ability of the π-bridge and donor, slow charge recombination and prevention of dye aggregation. To enhance the absorption ability of the multifunctional D–π core group, various thiophene derivatives,[31] which have widely been incorporated into organic sensitizers because of the effective conjugation and co-planarity relative to benzene moieties[32] as well as chemical stability and electronic tunability, were also introduced as the π-spacer between the **TBT** π-bridge and the A unit. Furthermore, to retard charge recombination with the electrolyte and to prevent dye aggregation, the dihexyloxyphenyl-substituted biphenylamine was used as the bulky donor group.[19.33] In this study, we employed thiophene derivatives as π-spacers, such as thiophene (**T**),[34] bithiophene (**BT**)[35,36] and thienothio[3,2-*b*]thiophene (**TT**),[15,37] for **SGT-121**, **SGT-123** and **SGT-125** (**Scheme 1**) in order to evaluate the effect of the π-spacer extension of the sensitizer on the optical properties and device performances.[38] **SGT-127** has no thiophene π-

spacer between the **TBT** π-bridge and the A unit so that the ability of the electron-rich thiophene unit could be evaluated. By controlling the optical and electrochemical properties of thiophene π-spacers, **SGT-123** containing the **BT** moiety exhibited a significantly enhanced photocurrent and voltage, simultaneously.

Results and Discussion

The synthetic routes for the new **TBT**-based organic sensitizers with the various thiophene derivatives as the π-spacers are illustrated in **Scheme 1**. The various thiophene derivatives as the π-spacers were introduced between the **TBT** π-bridge and the cyanoacrylic acid (**A**) of the D–π–A sensitizers, coded as the **T**, **BT** and **TT** moieties for **SGT-121**, **SGT-123** and **SGT-125**, respectively. For all **SGT** sensitizers, the starting material (**2**) was prepared by bromination using the *N*-bromosuccinimide (NBS) of **1** followed by the Buchwald–Hartwig C–N coupling reaction[39] between 6-bromothieno[3,2-*b*][1]benzothiophene[27] and the biphenylamine donor (**Scheme S1**). The aldehyde derivatives (**4**) were prepared through a Stille coupling reaction[40] of **2** with the tin derivative (**3)** of each protected aldehyde. The aldehyde derivative **5** for **SGT-127** was prepared through formylation using *n*-BuLi/N-formylpiperidine with **2** at low temperature. The final sensitizers of **SGT-121**, **SGT-123**, **SGT-125** and **SGT-127** were prepared through Knoevenagel condensation with cyanoacrylic acid.[41] The chemical structures of the final sensitizers were characterized by ^{1}H NMR, ^{13}C NMR and MALDI-TOF mass spectroscopies, and their corresponding characterisation data are summarized in the experimental section.

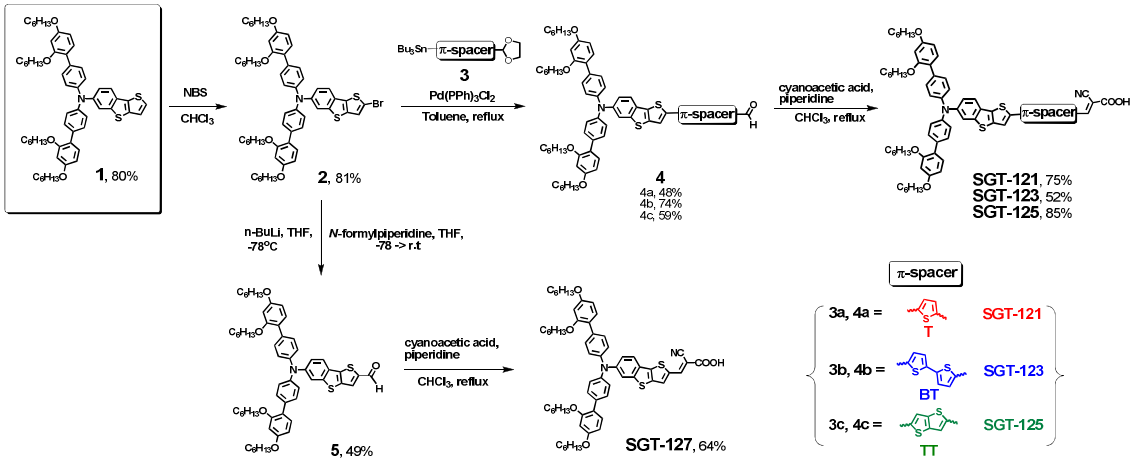

Scheme 1. Synthesis of **SGT-121**, **SGT-123**, **SGT-125** and **SGT-127**.

The absorption and emission spectra of the **SGT** sensitizers in THF are shown in **Figure 1a**, and the photophysical properties are summarized in **Table 1**. All of the sensitizers show two absorption wavelengths (λ_{max}) in the ranges of 300–400 and 400–600 nm, respectively. The former corresponds to the π–π* transition and the latter is attributed to intramolecular charge transfer (ICT) from D to A in the D–π–A sensitizer. The λ_{max} and molar extinction coefficient (ε) of thiophene-based sensitizers are known to increase with the extension of thiophene chain length.[15,37,38a,38c] Compared to **SGT-127**, the λ_{max} and ε values of **SGT-121**, **SGT-123** and **SGT-125** were red-shifted by 10, 15.5 and 8 nm, respectively, and were enhanced above 4×10^3 M^{-1} cm^{-1} in the 400–600 nm region, which is consistent with the insertion of electron-rich thiophene units.[38d] Although the ε value of planar, fused, **TT**-based **SGT-125** was higher than that of **SGT-121,** the λ_{max} of **SGT-125** is slightly blue-shifted by 2 nm with respect to **SGT-121,** despite increasing the π-spacer length from the **SGT-121** (2.52 Å) to **SGT-125** (4.62 Å). This can be explained by the dihedral angle (4.58°) of **SGT-125** between the **TBT** unit and the **TT** π-spacer being larger than that of **SGT-121** (1.39°), which disturbs charge transfer and results in the hypsochromic shift in absorption wavelength. Interestingly, the

longest π-conjugated **SGT-123** system exhibited the highest λ_{max} and ε value as well as the broadest absorption band,[36,38c,38d] indicating that the elongation of π-conjugation length may play as a key role in the absorption ability. The emission maximum (λ_{em}) of each sensitizer appeared at 588 (**SGT-127**), 621 (**SGT-125**), 625 (**SGT-121**) and 646 nm (**SGT-123**), which follows the same trend as that in the absorption spectra (**Figure 2a** and **Table 1**).

The electrochemical properties of sensitizers were investigated by cyclic voltammetry (CV) in water-free acetonitrile containing 0.1 M $TBAPF_6$ as the supporting electrolyte at room temperature (**Figure S2**), and the corresponding energy diagram is shown in **Figure 1b** with electrochemical data summarized in **Table 1**. The redox potentials (E_{OX}) of **SGT-121**, **SGT-123**, **SGT-125** and **SGT-127** correspond to the highest occupied molecular orbital (HOMO) energy levels located at 1.14, 1.1, 1.15 and 1.21 V vs. NHE, respectively, which are more positive than that of the Co^{2+}/Co^{3+} redox couple (0.59 V vs. NHE),[42] and thus offer sufficient driving forces for the regeneration of oxidized dyes. As thiophene π-spacers are inserted between **TBT** and **A**, the HOMO energy levels of **SGT-121, SGT-123** and **SGT-125** are upshifted by about 0.07, 0.11 and 0.06 V, respectively, leading to a decrease in their HOMO–LUMO energy gaps compared with **SGT-127.** Among them, **SGT-123**, with the longest π-conjugation length, shows the smallest band gap, which is favourable for the bathochromic shift in the absorption spectra, contributing to improvements in the photocurrent (J_{sc}). The lowest unoccupied molecular orbital (LUMO) energy levels of sensitizers were calculated using the equation of $E_{OX} - E_{0-0}$, where E_{0-0} is the zero–zero transition energy derived from the intersection of the normalized absorption and emission spectra. The LUMO energy levels (E_{OX}^*) of **SGT-121** to **SGT-127** are −1.18, −1.15, −1.17 and −1.21 V vs. NHE, which are more negative than the TiO_2 conduction band (E_{CB} = −0.5 V vs. NHE).[43] As shown in **Table 1**, the $E_{OX}^* - E_{CB}$ values, i.e., the driving forces (ΔG_{inj}) of the

sensitizers are sufficient for electron injection from the excited state of the sensitizers into the E_{CB} of TiO_2 to occur.[2] The E_{OX}^* of **SGT-127** without a thiophene π-spacer is clearly upshifted with respect to the other sensitizers, which causes the hypsochromic shift in the absorption spectrum and results in a low photocurrent. In contrast, **SGT-123** has a more positive E_{OX}^* value as well as a lower ΔG_{inj} than the other sensitizers, which can be expected to ensure better electron injection, higher photocurrent and efficiency.

To get an insight into the geometric and electronic properties of the sensitizers, density functional theory (DFT) calculations were performed using the Gaussian 09 program at the B3LYP/6-31G (d,p) level;[44] the HOMO and LUMO electron distributions are shown in **Figure 1b**. The HOMO is distributed along the donor part and the **TBT** π-bridge, whereas the LUMO is delocalized over the cyanoacrylic acid and thiophene π-spacer. This significant charge separation within the sensitizers can also result in efficient electron injection upon photoexcitation. In addition, as all sensitizers have similar dihedral angles (>40°) between the *N* atom of the amine donor and the **TBT** π-bridge, the thiophene π-spacer lengths and their dihedral angles can have important roles in the electronic communication between the **TBT** π-bridge and the **A** (**Figure S1**).

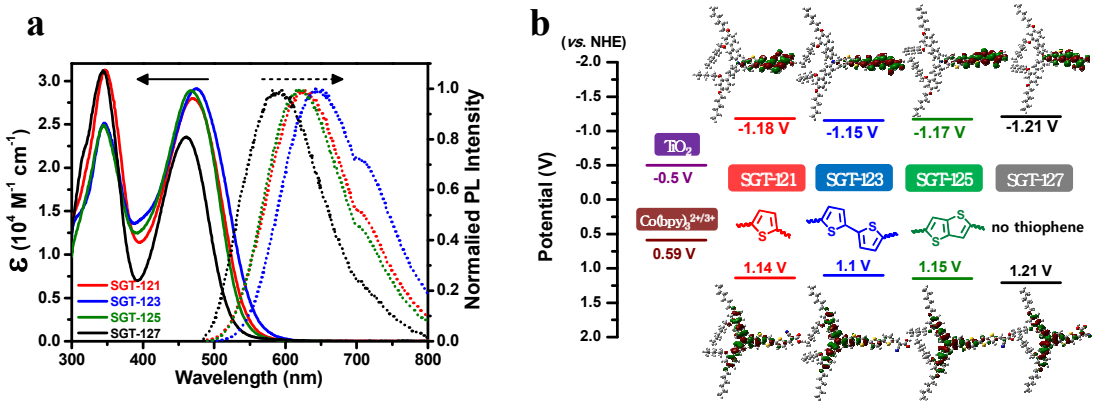

Figure 1. (a) UV/Vis absorption and emission spectra of the **SGT** sensitizers measured in THF. (b) Calculated frontier molecular orbitals and experimental energy-level diagram of the **SGT** sensitizers.

Table 1. Photophysical and electrochemical properties of the **SGT** sensitizers.

Dye	$\lambda_{abs\ max}$ (nm)[a]	ε ($M^{-1}\ cm^{-1}$)	$\lambda_{em\ max}$ [a] (nm)	$E_{0\text{-}0}$ [b] (eV)	E_{OX} [c] (V *vs.* NHE)	E_{OX}^{*} [d] (V *vs.* NHE)	ΔG_{inj} [e] (eV)	θ [f] (°)
SGT-121	347 469	31227 28007	625	2.30	1.14	−1.18	0.68	1.39
SGT-123	345.5 474.5	25066 29125	646	2.25	1.10	−1.15	0.65	10.28
SGT-125	345 467	26918 28898	621	2.32	1.15	−1.17	0.67	4.58
SGT-127	344 459	31185 23474	588	2.42	1.21	−1.21	0.71	-

[a]Absorption and emission spectra were measured in THF
[b]E_{0-0} was determined from the intersection of absorption and emission spectra in THF
[c]Oxidation potentials of dyes on TiO_2 were measured in CH_3CN with 0.1M $TBAPF_6$ and a scan rate of 50 mV s^{-1} (calibrated with Fc/Fc^+ as an external reference and converted to NHE by addition of 0.63V)
[d]Excited-state oxidation potentials were calculated according to $E_{ox} - E_{0-0}$
[e]Driving force for electron injection from the E_{ox}^{*} to the E_{CB} of TiO_2 (−0.5 V vs. NHE)
[f]Dihedral angle between TBT unit and thiophene π-spacer

To understand the difference of IPCE maximum fluctuation for all SGT sensitizers, the electron injection efficiency (η_{inj}) was measured for dye-coated Al_2O_3 and TiO_2 films by the time-resolved photoluminescence (TR-PL) (**Figure 2).**[44] The measured PL signal intensity (I_{PL}) was fitted by three exponentials, $I_{PL} = A_1 \exp(-t/\tau_1) + A_2 \exp(-t/\tau_2) + A_3 \exp(-t/\tau_3)$. For all of the sensitizers, the TiO_2 film shows significantly faster PL decay than the Al_2O_3 film, because electron injection occurs at the TiO_2/dye interface but not at the Al_2O_3 interface (**Figure 2**). Therefore, the PL decays of the Al_2O_3 films provide the lifetimes of the sensitizers themselves, whereas the PL decays of the TiO_2 films give information about the dynamics of electron injection. As the structural heterogeneity of film samples often gives rise to multi-exponential PL decay, we calculated the amplitude-weighted average lifetimes

(τ_{av}) of the PL decays in order to simplify the comparison between the PL decays of various samples, as summarized in **Table 2**. We calculated η_{inj} using the equation of $\eta_{inj} = 1-(\tau_{TiO_2})/(\tau_{Al_2O_3})$. The calculated η_{inj} values of **SGT-121**, **SGT-123**, **SGT-125** and **SGT-127** were 91.2, 98.4, 91.9 and 83.8%, respectively. We can see that η_{inj} increases in the order of **SGT-127** < **SGT-121** < **SGT-125** < **SGT-123**, indicating that the E_{OX}^{*} value is positively shifted by the insertion of thiophene π-spacers. Considering the significant difference of η_{inj} values, we can expect that the electron injection efficiency (η_{inj}) has effect on the IPCE variation and device performance in our DSSCs.

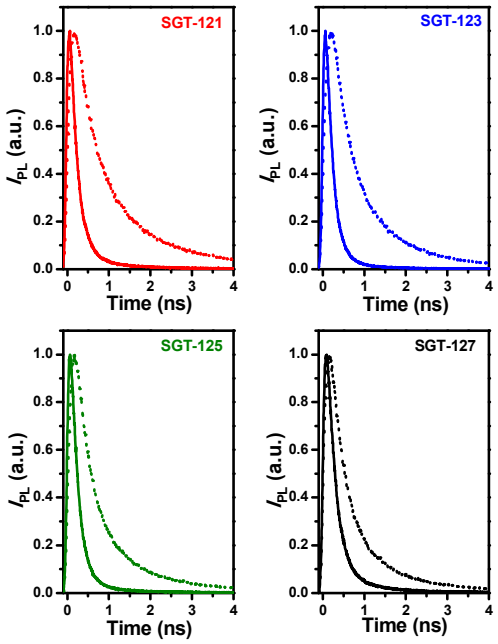

Figure 2. TR-PL decay traces of dye-adsorbed mesoporous Al_2O_3 (dotted line) and TiO_2 films (solid line) for **SGT-121** (red), **SGT-123** (blue), **SGT-125** (green) and **SGT-127** (black). Excitation wavelength: 393 nm; detection wavelength: $\lambda_{em\ max}$ of each sensitizer.

Table 2. Fit parameters of the PL decays shown in **Figure 2** and the calculated electron injection efficiencies.

		τ_1 (ns)	A_1	τ_2 (ns)	A_2	τ_3 (ns)	A_3	$\langle\tau\rangle_{av}$ [a] (ns)	η_{inj} (%)
SGT-121	Al_2O_3	3.82	1.9	1.143	33.8	0.2437	64.3	0.619	91.2
	TiO_2	1.246	0.4	0.243	6.2	0.0367	93.4	0.054	
SGT-123	Al_2O_3	3.666	1.2	1.015	32.7	0.2802	66.1	0.561	98.4
	TiO_2	1.041	0.0	0.195	0.7	0.0076	99.3	0.009	
SGT-125	Al_2O_3	3.258	1.7	0.903	24.7	0.2060	73.6	0.430	91.9
	TiO_2	0.857	0.3	0.176	5.0	0.0246	94.7	0.035	
SGT-127	Al_2O_3	2.684	2.2	0.716	23.8	0.1522	74.0	0.343	83.8
	TiO_2	0.931	0.9	0.211	9.5	0.0304	89.6	0.056	

[a]The values of τ_{av} were determined using the equation $\langle\tau\rangle_{av} = A_1\tau_1 + A_2\tau_2 + A_3\tau_3$.

On the basis of in-depth optical and electrochemical evaluations of the sensitizers, their photovoltaic performances were evaluated in $Co(bpy)_3^{2+/3+}$ (bpy=2,2'-bipyridine), exhibiting a higher open-circuit voltage (V_{oc}) than the traditional I^-/I_3^- redox couple;[42] the DSSC fabrication details are described in the **SI.** The current–voltage (J–V) and incident photon-to-current conversion efficiency (IPCE) curves are shown in **Figures 3a** and **3b**, with the photovoltaic parameters summarized in **Table 3**. Clearly, DSSCs based on **SGT-121**, **SGT-123** and **SGT-125** significantly increased in terms of J_{sc} to over 14 mA cm^{-2} compared to **SGT-127** without a π-spacer (8.67 mA cm^{-2}), which is attributed to the increased light-harvesting ability (LHE) of the electron-rich thiophene unit.[15,36,37,38a] The J_{sc} values of the DSSCs increased in the order of elongation of the π-spacer length, which is consistent with the absorption and IPCE spectra (**Figure 1a** and **Figure 3b**). As shown in **Figure 3b**, the IPCE onsets and maximum IPCE values increase in the same order as J_{sc}, which is enough to prove the enhanced J_{sc} of all **SGT** sensitizers, according to the additional difference in the amount of dye adsorbed on the TiO_2 surface (**Table 3**). The **SGT-123**-based DSSC exhibited

the highest performance (J_{sc}, V_{oc}, fill factor (*FF*) and PCE = 16.16 mA cm^{-2}, 830 mV, 0.72 and 9.69%, respectively), whose values are much higher than those of **SGT**-series sensitizers (**Table 3**).

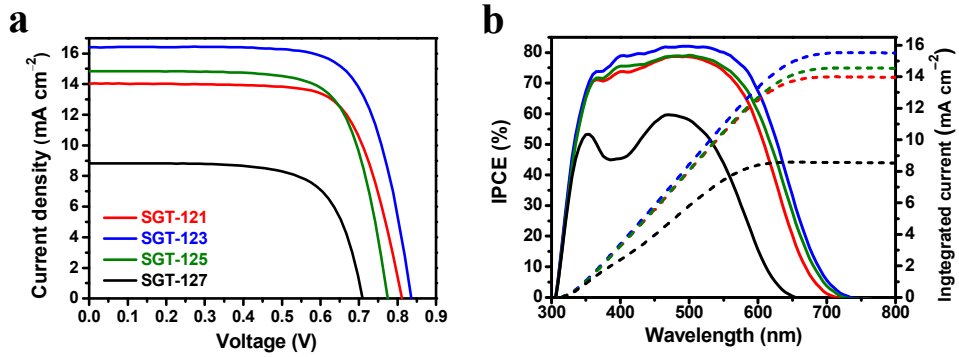

Figure 3. (a) Current–voltage (*J*–*V*) characteristics of the DSSCs measured under one sun illuminated AM 1.5G. The TiO_2 film thickness is 5.5 μm for the active layer and 3.3 μm for the scattering layer. (b) The corresponding IPCE spectra.

Table 3. Photovoltaic performances of the DSSCs based on the various sensitizers under one sun illumination (AM 1.5G) (mean of three DSSCs).

Dye[a]	Adsorption amount (10^{-7} mol cm^{-2})	J_{sc} (mA cm^{-2})	V_{oc} (mV)	*FF* (%)	PCE[b] (%)
SGT-121	0.99	14.00 ± 0.09	809 ± 4.7	72.71 ± 0.74	8.24 ± 0.06
SGT-123	1.48	16.16 ± 0.57	830 ± 3.2	72.09 ± 0.15	9.69 ± 0.35
SGT-125	1.32	14.74 ± 0.15	773 ± 1.4	71.86 ± 0.58	8.20 ± 0.16
SGT-127	0.91	8.67 ± 0.17	707 ± 5.0	70.45 ± 1.17	4.32 ± 0.05

[a]Dipping solution: 0.3 mM dye solution (EtOH/THF = 2:1) with 20 mM CDCA.
[b]Irradiated light: AM 1.5G (100 mW cm^{-2}); cell area tested with a metal mask: 0.141 cm^2.
Cobalt electrolyte: 0.22 M $Co^{II}(bpy)_3](BCN)_4)_2$, 0.05 M $[Co^{III}(bpy)_3](BCN)_4)_3$, 0.1 M $LiClO_4$ and 0.8 M TBP in acetonitrile (ACN).

Most of the reported photovoltaic performances of DSSCs with thiophene-based sensitizers in the I^-/I_3^- redox electrolyte show an increase in J_{sc} with the extension of π-conjugation length, whereas their V_{oc} values decrease with the opposite trend.[38a,38d,46] Unlike this tendency,

the V_{oc} values for our sensitizer-based DSSCs employing the $Co(bpy)_3^{2+/3+}$ redox couple increase in the order of **SGT-127** (707 mV) < **SGT-125** (773 mV) < **SGT-121** (809 mV) < **SGT-123** (830 mV). In general, the V_{oc} is dependent upon the difference between the quasi-Fermi level of TiO_2 (E_{Fn}) and the redox potential of the electrolyte (E_{ox}).[47] Considering that the same $Co(bpy)_3^{2+/3+}$ redox electrolyte was used for all of the DSSCs, the V_{oc} may be determined by the E_{Fn} of TiO_2, which is related to the position of the TiO_2 conduction band (E_{CB}) and the electron density in TiO_2.[48] In order to demonstrate these differences in V_{oc} values in the DSSCs, we conducted several electrochemical measurements using electrochemical impedance spectroscopy (EIS), density of occupied trap states (DOS) of dye-coated TiO_2, intensity-modulated photovoltage spectroscopy (IMVS) and intensity-modulated photocurrent spectroscopy (IMPS); see also **Figure S3** for an extended discussion.

The EIS of the DSSCs was measured under a –0.79 V applied bias voltage in the dark, except for the **SGT-127**-based DSSC (–0.74 V) with the lower V_{oc}. Nyquist and Bode plots are shown in **Figures 4a** and **4b,** and the EIS data estimated with an appropriate equivalent circuit (EC)[49] are listed in **Table 4**. In the Nyquist plots (**Figure 4a**), the three semicircles located in the high-, middle- and low-frequency regions are assigned to the charge-transfer resistance (R_{ct}) at the Pt/electrolyte interface, the charge recombination resistance (R_{rec}) at the TiO_2/dye/electrolyte interface and mass transport of the redox couple in the bulk electrolyte solution, respectively.[50] With the large radius of the middle semicircle, the R_{rec} values increased in the order of **SGT-125** (27.3 Ω) < **SGT-121** (27.97 Ω) < **SGT-123** (83.73 Ω) (**Table 4**), indicating that the **SGT-123**-based DSSC can retard charge recombination more efficiently than the other sensitizers, resulting in the highest V_{oc}. Furthermore, the capacitance (C_μ) at the TiO_2/dye/electrolyte interface can also significantly affect the V_{oc} of DSSCs, owing to the E_{CB} shift of TiO_2.[51] The difference in the C_μ was slight, but it decreased in the

order of **SGT-123** > **SGT-121** > **SGT-125**, implying an upshift in the E_{CB}. The electron lifetimes (τ_r) estimated by $\tau_r = C_\mu \cdot R_{rec}$ were 9.65 (**SGT-121**), 29.66 (**SGT-123**), 9.57 (**SGT-125**) and 10.56 ms (**SGT-127**), which is in agreement with the observed V_{oc} values for **SGT-123** (830 mV), **SGT-121** (809 mV), **SGT-125** (773 mV) and **SGT-127** (707 mV). This trend could be also confirmed in the mid-frequency region of the Bode phase plot (**Figure 4b**). The longer electron lifetime of **SGT-123** compared to the other sensitizers is associated with more effective suppression of the back reaction of the injected electron with $Co(bpy)_3^{3+}$ in the electrolyte, leading to a higher V_{oc} and improved device efficiency. Moreover, the photovoltaic performance can be confirmed by the charge-collection efficiency (η_{cc}) derived from $\eta_{cc} = (1 + R_{tr}/R_{rec})^{-1}$ or $\eta_{cc} = (1 + \tau_n/\tau_r)^{-1}$.[41a,47] The η_{cc} values of the DSSCs calculated from the above EIS parameters are shown in **Figure 4c** and **Table 4**. The comparatively high R_{rec} value observed for **SGT-123** can retard charge recombination, resulting in an increased η_{cc} of the DSSC. The calculated η_{cc} values for **SGT-121**, **SGT-123**, **SGT-125** and **SGT-127** were equal to be 95.22, 97.23, 94.36 and 93.7%, respectively. Moreover, the electron transport, recombination time and η_{cc} values of all DSSCs were also obtained from IMVS and IMPS measurements (**Figure S3**), which were in good agreement with the EIS results.

To further investigate the differences in V_{oc} with changes in the trap state induced by each sensitizer, CV was performed for each **SGT** sensitizer-absorbed TiO_2 electrode with CDCA in 0.1 M $LiClO_4$ and acetonitrile (**Figure S4**). **Figure 4d** shows the capacitive currents of the different electrodes at the $TiO_2/LiClO_4$ interface, which exhibited gradual onsets under a forward potential. The distribution of the trap states can be estimated from the density of states (DOS) calculation: $DOS=(dQ/dV)(N_A/F)$,[51] where Q is the total number of surface trapping sites, N_A is Avogadro's number, F is the Faraday constant and V is the potential applied to the electrode. Compared with the onsets of the capacitive currents, the onsets move

upwards in the order of **SGT-127** (−0.212 V) < **SGT-125** (−0.224 V) < **SGT-121** (−0.242 V) < **SGT-123** (−0.261 V), indicating that the upshift of E_{CB} in the above order can contribute to the increase in the V_{oc}.[48] Therefore, the highest V_{oc} of the **SGT-123**-based DSSC can be explained by the negative shift in the E_{Fn} level of its electrode. Considering all factors for the V_{oc} differences, the enhancement of V_{oc} can be caused either by a negative shift in the E_{CB} or the retarded recombination of the injected charge in TiO_2.[47a,48,53] In this respect, both the slower charge-recombination rate observed by EIS and IMVS analyses (**Figure 4**) and the negative shift in the E_{CB} according to the DOS results (**Figure 4d**) influence the increase in V_{oc} for the **SGT-123**-based DSSC. The V_{oc} of the **SGT-125** based DSSC decreased by 36 mV compared to **SGT-121**, which can be explained by the strong aggregation of introduced **TT** π-spacer.[31c] The V_{oc} results also suggest that the π-conjugation length of the sensitizers can slightly impact dye adsorption and suppress the recombination by complex formation with the redox electrolyte.[54] Thus, the longest π-conjugation length of **SGT-123** can decrease **the** recombination possibility between the charge and the $Co(bpy)_3^{3+}$ ion, which results in an enhancement of the V_{oc}.[23]

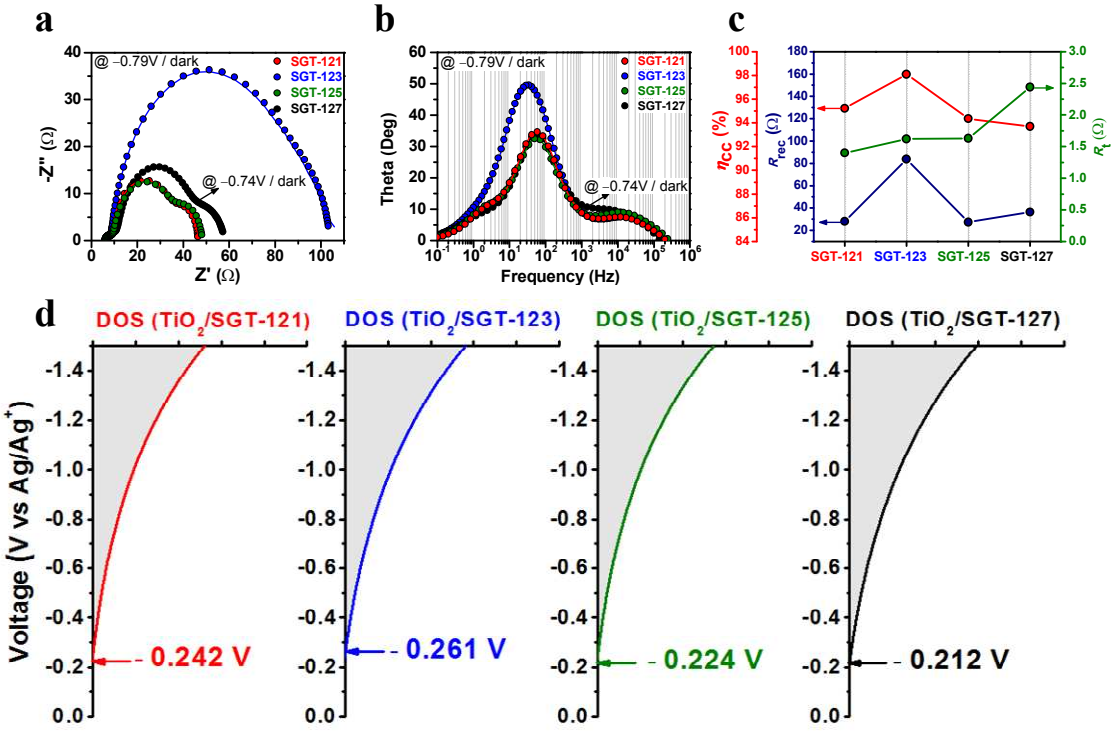

Figure 4. (a) Nyquist and (b) Bode plots obtained from the DSSCs based on the various sensitizers in the dark with a forward bias of –0.79 V, except for SGT-127 (–0.74 V). (c) Charge-collection efficiency (η_{cc}) of the DSSCs according to EIS measurements. (d) The exponential distribution of the DOS deduced by plotting the capacitive charge of electrons in the surface states versus the applied potential for the TiO_2/SGTs/CDCA electrodes. The capacitive charging current at a negative potential is attributed to the filling of surface states below the conduction band edge of TiO_2 for all structures**.**

Table 4. EIS, IMVS and IMPS parameters for the DSSCs based on various **SGT** sensitizers.

Device	EIS[a]						IMVS & IMPS		
	R_{tr} (Ω)	R_{rec} (Ω)	C_μ (mF)	τ_n (ms)	τ_r (ms)	η_{cc} (%)	τ_r (ms)	τ_n (ms)	η_{cc} (%)
SGT-121	1.40	27.97	0.34	0.48	9.65	95.22	34.94	5.95	82.67
SGT-123	2.36	83.73	0.36	0.84	29.66	97.23	38.08	5.40	85.43
SGT-125	1.63	27.3	0.35	0.57	9.57	94.36	22.19	4.46	79.42
SGT-127	2.44	36.38	0.29	0.70	10.56	93.70	50.14	11.14	77.88

[a]Values calculated from EIS data measured at a forward bias of –0.79 V (–0.74 V for **SGT-127**) under dark conditions. R_{tr}: transport resistance; R_{rec}: charge-recombination resistance; C_μ: chemical capacitance; τ_n: transport time; τ_r: electron lifetime; η_{cc}: charge-collection efficiency.

To obtain insights into the mass-transport limitation of $Co(bpy)_3^{3+}$ ions and the recombination kinetics, photocurrent transients[55] and open-circuit voltage decay (OCVD) measurements[56] were recorded for the complete DSSCs. As shown in **Figure 5a**, the ratio of the initial peak current to the steady-state current in the photocurrent transients slightly decreased in the order of **SGT-123** > **SGT-121** > **SGT-125** > **SGT-127**, indicating that the retarded mass transport can also lead to losses in the photocurrents and the DSSC performances. As can be seen in **Figure 5b**, after 1 s of illumination, the V_{oc} of the **SGT-127**-based DSSC exhibited a sharp decay, owing to fast electron recombination related to the electron lifetime. On the other hand, the V_{oc} of the DSSC based on **SGT-123** showed remarkably slower decay rates relative to the other DSSCs, which means a slower recombination rate and a longer electron lifetime. In other words, there were more electrons surviving the back-reactions in the DSSC based on **SGT-123** (inset in **Figure 5b**).

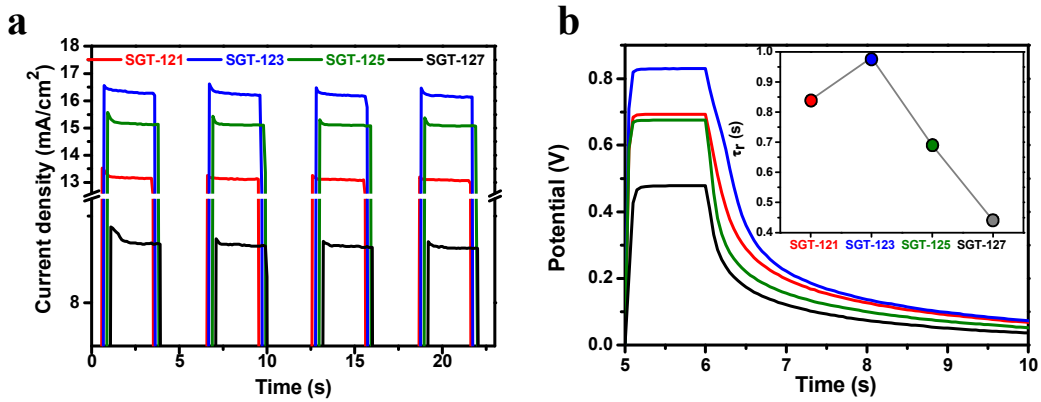

Figure 5. (a) Photocurrent transient dynamics of the DSSCs with various sensitizers. (b) Open-circuit voltage decay (OCVD) curves for the same DSSCs. The inset shows the electron lifetimes of the same DSSCs.

Conclusions

A series of sensitizers based on the π-spacer units of thiophene derivatives, e.g., thiophene (**T**), bithiophene (**BT**) and thienothio[3,2-*b*]thiophene (**TT**) moieties, containing dihexyloxyphenyl-substituted biphenylamine as an electron donor, thieno[3,2-*b*][1]benzothiophene (**TBT**) as the new fused π-bridge and cyanoacrylic acid as acceptor/anchor, has been specifically developed as **SGT-121**, **SGT-123** and **SGT-125** for high-efficiency DSSCs. We evaluate the effect of extended thiophene π-spacers in D–π–A organic sensitizers on the absorption, energy levels and photovoltaic performances of the sensitizers compared with **SGT-127** without thiophene, which acts as the reference sensitizer. It is found that the electronic distributions of all **SGT** sensitizers exhibit good charge separation between the HOMO and LUMO energy levels. On the other hand, the extension of the π-spacer length close to the acceptor group clearly red-shifts the absorption band, increases the molar extinction coefficients and positively shifts the LUMO levels compared to **SGT-127**, which leads to enhanced DSSC performances. The photovoltaic performances of **SGT** sensitizers are investigated in the $Co(bpy)_3^{2+/3+}$ (bpy=2,2'-bipyridine) redox couple, exhibiting a higher V_{oc} than in the I^-/I_3^- electrolyte. As the π-conjugation length of the sensitizer is increased, the J_{sc} and IPCE onset values are enhanced in the order of the π-conjugation length. From the results of EIS, DOS and IMVS analyses, the **SGT-123**-based DSSC exhibits the highest V_{oc}, indicating a slower charge-recombination rate and a negative shift of the E_{CB} of TiO_2. Consequently, the DSSC based on **SGT-123** containing **BT** shows the best performance with a PCE of 9.69%, J_{sc} of 16.16 mA cm^{-2}, V_{oc} of 830 mV and *FF* of 0.72, which are much higher than those of the **SGT-127** reference sensitizer (4.32%, 8.67 mA cm^{-2}, 707 mV and 70.45%). These structure–performance relationships provide valuable information for the modification of thiophene-based π-spacers in organic sensitizers.

Experimental section

Materials and Synthesis

All reactions were carried out under a nitrogen atmosphere. Solvents were distilled from appropriate reagents. All reagents were purchased from Sigma–Aldrich, TCI and Alfar Aesar. 6-Bromothieno[3,2-*b*][1]benzothiophene,[27] bis(2',4'-dihexyloxybiphenyl-4-yl)-amine,[19] [5-(1,3-dioxolan-2-yl)thiophen-2-yl]tributylstannane (**3a**),[57] [5′-(1,3-dioxolan-2-yl)-2,2′-bithiophen-5-yl]tributylstannane (**3b**)[58] and [5-(1,3-dioxolan-2-yl)thieno[3,2-*b*]thiophen-2-yl]tributylstannane (**3c**)[59] were synthesized according to previous reports, but with slight modification. The synthetic routes for SGT-121, SGT-123, SGT-125 and SGT-127 are showed in **Scheme 1** and the details can be depicted as follows.

***N,N*-Bis(2',4'-dihexyloxybiphenyl-4-yl)-thieno[3,2-*b*][1]benzothiophen-6-amine (1)** [27]

Bis(2',4'-dihexyloxybiphenyl-4-yl)-amine (0.402g, 0.56 mmol), 6-bromothieno[3,2-*b*][1]benzothiophene (0.15 g, 0.56 mmol), $Pd_2(dba)_3$ (0.02 g, 0.02 mmol), P(*t*-Bu)$_3$ (0.01 ml, 0.02 mmol), and sodium tert-butoxide (0.57g, 5.91 mmol) in dry toluene (15 ml) was heat to reflux for 1 hr. After cooling to room temperature, saturated ammonium chloride solution was added to the reaction solution. The solvent was removed by rotary evaporation, and the crude product was purified by column chromatography on silica gel with CH_2Cl_2/*n*-hexane (*v*/*v*, 1:3) as eluent to afford **1** as a yellow sticky solid (0.4 g, 80%). ^{1}H NMR (300 MHz, $CDCl_3$) δ 7.73 (d, *J* = 8.4 Hz, 1 H), 7.62 (s, 1H), 7.41-47 (m, 5 H), 7.27-7.30 (m, 4 H), 7.15-7.17 (d, 4 H), 6.52-6.55 (m, 4 H), 3.94-4.01 (q, 8H), 1.84 (m, 8H), 1.28-1.50 (m, 24H), 0.91 (m, 12H). ^{13}C NMR (300 MHz, $CDCl_3$): *δ* 159.6, 157.05 146.0, 145.2, 144.1, 137.2, 134.8, 133.0, 130.9, 130.3, 128.0, 127.0, 123.5, 122.9, 122.5, 121.3, 120.4, 119.1, 105.3, 100.4, 68.4, 31.7, 29.4, 25.9, 22.7, 14.1. MS (MALDI-TOF) *m/z* calculated for $C_{58}H_{71}NO_4S_2$: 910.3186; found, 909.2919.

_N,N_-Bis(2',4'-dihexyloxybiphenyl-4-yl)-2-bromothieno[3,2-*b*][1]benzothiophen-6-amine (2) [27]

The compound **1** (0.68 g, 0.75 mmol) was dissolved in 100 mL of chloroform. *N*-bromosuccinimide (0.13 g, 0.75 mmol) was added in one portion. A mixture was stirred for 1 hr and the mixture was poured into water. Aqueous was extracted with dichloromethane and the combined organic layer was dried over anhydrous $MgSO_4$. The solvent was removed by rotary evaporation, and the crude product was purified by column chromatography on silica gel with CH_2Cl_2/*n*-hexane (*v*/*v*, 1:2) as eluent to afford **2** as a yellow sticky solid (0.6 g, 81%). ^{1}H NMR (300 MHz, $CDCl_3$) δ 7.65 (m, 2 H), 7.49-52 (d, 6 H), 7.27-7.33 (m, 4 H), 7.19-21 (d, J = 8.4 Hz, 4 H), 6.56 (m, 4 H), 4.01 (q, 8H), 1.91 (m, 8H), 1.33-1.49 (m, 24H), 0.91 (m, 12H). ^{13}C NMR (300 MHz, $CDCl_3$): δ 159.6, 156.9, 1445.8, 145.7, 145.4, 142.9, 135.6, 134.9, 134.0, 133.1, 130.9, 130.3, 127.4, 123.7, 123.1, 122.3, 121.1, 118.4, 112.8, 105.2, 100.3, 68.3, 31.7, 29.4, 25.8, 22.7, 14.1.

[5-(1,3-Dioxolan-2-yl)thiophen-2-yl]tributylstannane (3a)

Compound **3a** was synthesized according to previously reported methods.[57] ^{1}H NMR (300 MHz, $CDCl_3$): δ 7.27–7.28 (d, J = 3.3 Hz, 1 H), 7.04–7.05 (d, J = 3.3 Hz, 1 H), 6.15 (s, 1 H), 4.13–4.16 (m, 2 H), 4.01–4.04 (m, 2 H), 1.50–1.58 (m, 6 H), 1.29–1.36 (m, 6 H), 1.06–1.11 (m, 6 H), 0.86–0.92 (m, 9 H).

[5′-(1,3-Dioxolan-2-yl)-2,2′-bithiophen-5-yl]tributylstannane (3b)

Compound **3b** was synthesized according to previously reported methods.[58] ^{1}H NMR (300 MHz, $CDCl_3$): δ 7.26–7.27 (d, J = 3.3 Hz, 1 H), 6.99–7.05 (m, 3 H), 6.07 (s, 1 H), 4.12–4.14 (m, 2 H), 3.99–4.04 (m, 2 H), 1.52–1.65 (m, 6 H), 1.28–1.38 (m, 6 H), 1.08–1.13 (m, 6 H), 0.87–0.93 (m, 9 H).

[5-(1,3-Dioxolan-2-yl)thieno-3,2-b-thiophen-2-yl]tributylstannane (3c)

Compound **3c** was synthesized according to previously published reports.[59] ^{1}H NMR (300 MHz, $CDCl_3$): δ 7.34–7.36 (d, 1 H), 7.23–7.24 (d, 1 H), 6.16 (s, 1 H), 4.12–4.16 (m, 2 H), 4.00–4.05 (m, 2 H), 1.54–1.63 (m, 6 H), 1.28–1.37 (m, 6 H), 1.10–1.15 (m, 6 H), 0.87–0.93

(m, 9 H).

5-(6-[Bis(2',4'-dihexyloxybiphenyl-4-yl)amino]thieno[3,2-*b*][1]benzothiophen-2-yl)thiophene-2-carbaldehyde (4a)

A mixture of compound **2** (0.1 g, 0.10 mmol), **3a** (0.05g, 0.11 mmol) and $Pd(PPh_3)_2Cl_2$ (0.01 g, 0.01 mmol) in dry toluene (20 mL) was heated at 110°C for 12 h under an inert N_2 atmosphere. After complete consumption of the starting materials, dilute hydrochloric acid was added and the mixture was stirred at room temperature for 10 min and extracted with dichloromethane. The organic phase was washed in brine, dried over $MgSO_4$ and the solvent was evaporated under vacuum. The crude product was purified by column chromatography on silica gel with CH_2Cl_2/*n*-hexane (v/v, 1:1) to afford **4a** as a yellow sticky solid (0.05 g, 48%). ^{1}H NMR (300 MHz, $CDCl_3$): δ 9.87 (s, 1H), 7.69 (d, J = 5.2 Hz, 1 H), 7.67 (s, 1H), 7.58 (d, J = 1.8 Hz, 1 H), 7.53 (d, 1 H), 7.51 (s, 1 H), 7.45–7.48 (d, J = 8.7 Hz, 4 H), 7.30–7.82 (m, 3 H), 7.15–7.18 (d, J = 8.7 Hz, 4 H), 6.53 (m, 4H), 3.94 (q, 8H), 1.73–1.82 (m, 8H), 1.29–1.50 (m, 24H), 0.86 (m, 12H).

5-(6-[Bis(2',4'-dihexyloxybiphenyl-4-yl)amino]thieno[3,2-*b*][1]benzothiophen-2-yl)-2,2′-bithiophene-5-carbaldehyde (4b)

The synthetic procedure for **4b** was similar to that for **4a**, except that compound **3b** (0.06 g, 0.12 mmol) was used instead of **3a**. After complete consumption of the starting materials, dilute hydrochloric acid was added and the mixture was stirred at room temperature for 10 min and extracted with dichloromethane. The organic phase was washed in brine, dried over $MgSO_4$ and the solvent was evaporated under vacuum. The crude product was purified by column chromatography on silica gel with CH_2Cl_2/*n*-hexane (v/v, 2:1) to afford **4b** (0.09 g, 74%). ^{1}H NMR (300 MHz, $CDCl_3$): δ 9.83 (s, 1H), 7.63 (d, 1 H), 7.62 (s, 1H), 7.58 (d, J = 1.8 Hz, 1 H), 7.45–7.47 (d, J = 6.9 Hz, 4 H), 7.32 (s, 1 H), 7.23–7.25 (m, 4 H), 7.19 (d, 2 H), 7.14 (m, 4H), 6.54 (m, 4H), 3.95 (q, 8H), 1.72–1.81 (m, 8H), 1.27–1.50 (m, 24H), 0.88 (m, 12H).

5-(6-[Bis(2',4'-dihexyloxybiphenyl-4-yl)amino]thieno[3,2-*b*][1]benzothiophen-2-yl)thieno[3,2-b]thiophene-2-carbaldehyde (4c)

The synthetic procedure for **4c** was similar to that for **4a**, except that compound **3c** (0.07 g,

0.13 mmol) was used instead of **3a**. After complete consumption of the starting materials, dilute hydrochloric acid was added and the mixture was stirred at room temperature for 10 min and extracted with dichloromethane. The organic phase was washed in brine, dried over $MgSO_4$ and the solvent was evaporated under vacuum. The crude product was purified by column chromatography on silica gel with CH_2Cl_2/*n*-hexane (v/v, 2:1) to afford **4c** (0.07 g, 59%). ^{1}H NMR (300 MHz, $CDCl_3$): δ 9.92 (s, 1H), 7.66 (d, 1 H), 7.59 (d, 1H), 7.43–7.48 (m, J = 8.7 Hz, 6 H), 7.27–7.34 (m, 4 H), 7.19 (d, J = 8.7 Hz, 4 H), 6.55 (m, 4 H), 3.97 (q, 8H), 1.71–1.80 (m, 8H), 1.28–1.48 (m, 24H), 0.89 (m, 12H).

5-[6-Bis(2',4'-dihexyloxybiphenyl-4-yl)amino]thieno[3,2-*b*][1]benzothiophene-2-carbaldehyde (5)

n-BuLi (0.06 mL, 2.5 M in *n*-hexane) was added drop-wise to a solution of compound **2** (0.106 g, 0.11 mmol) in anhydrous THF (50 mL) at −78°C under a N_2 atmosphere. The reaction was kept at −78°C for 1 h. Then, *N*-formylpiperidine (0.02 mL, 0.21 mmol) was added, the mixture was allowed to warm to room temperature and stirred overnight. The solution was extracted with ether and the combined organic layers were dried over anhydrous Na_2SO_4 before being evaporated to dryness. The residue was purified by chromatography on silica gel, eluting with CH_2Cl_2/hexane(v/v, 1/2) to afford **5** as a yellow sticky solid (50mg, 49%). ^{1}H NMR (300 MHz, $CDCl_3$) δ 9.95 (s, 1H), 7.91 (s, 1 H), 7.792 (d, J = 8.4 Hz, 1H), 7.44-7.55 (m, 6 H), 7.17 (d, J = 8.4 Hz, 6 H), 6.55 (m, 4 H), 3.95 (q, 8H), 1.71-1.82 (m, 8H), 1.29-1.49 (m, 24H), 0.88 (m, 12H).

3-[5-(6-[Bis(2',4'-dihexyloxybiphenyl-4-yl)amino]thieno[3,2-*b*][1]benzothiophen-2-yl)thiophene-2-yl]-2-cyanoacrylic acid (SGT-121)

Compound **4a** (0.05 g, 0.05 mmol), dissolved in $CHCl_3$ (6 mL) and acetonitrile (6 mL), was condensed with 2-cyanoacetic acid (0.01g , 0.17 mmol) in the presence of piperidine (0.01 g, 0.17mmol). The mixture was refluxed for 12 h. After cooling the solution, the organic layer was removed in vacuo. The red solid of **SGT-121** was obtained by silica gel chromatography [CH_2Cl_2/ MeOH (v/v, 10:1)]. Yield: 75% (40 mg). M.p.: 171–173 °C. ^{1}H NMR (300 MHz, $CDCl_3$) δ 8.31 (s, 1H), 7.74 (d, J = 8.7 Hz, 1 H), 7.69 (d, 1H), 7.60 (s, 1 H), 7.57 (d, 1 H), 7.52 (s, 1 H), 7.46-7.49 (d, J = 8.7 Hz, 4 H), 7.28-7.34 (m, 3 H), 7.16-7.19 (d, J = 8.7 Hz, 4 H), 6.53 (m, 4H), 3.94 (q, 8H), 1.73-1.80 (m, 8H), 1.25-1.48 (m, 24H), 0.86 (m, 12H). ^{13}C NMR (300 MHz, DMSO-d_6) δ 162.1, 159.2, 157.7, 156.2, 145.1, 145.1, 143.6,

141.0, 139.9, 137.9, 136.4, 136.1, 133.5, 130.5, 130.2, 127.4, 124.8, 123.2, 122.3, 121.8, 119.6, 119.4, 111.5, 110.7, 109.5, 105.9, 100.2, 67.8, 67.5, 31.0, 30.8, 29.0, 28.7, 28.5, 25.2, 22.1, 22.0, 13.9, 13.8. UV-vis (THF, nm): λ_{max} (ε) 337 (38 356), 470.5 (28 080). PL (THF, nm): λ_{max} 626.MS (MALDI-TOF) *m/z* calculated for $C_{66}H_{74}N_2O_6S_3$: 1086.4986; found, 1086.3811.

3-[5-(6-[Bis(2',4'-dihexyloxybiphenyl-4-yl)amino]thieno[3,2-*b*][1]benzothiophen-2-yl)-2,2′-bithiophene-5-yl]-2-cyanoacrylic acid (SGT-123)

Compound **4b** (0.09 g, 0.08 mmol), dissolved in $CHCl_3$ (9 mL) and acetonitrile (9 mL), was condensed with 2-cyanoacetic acid (0.02 g, 0.29 mmol) in the presence of piperidine (0.02 g, 0.28mmol). The mixture was refluxed for 12 h. After cooling the solution, the organic layer was removed in vacuo. The red solid of **SGT-123** was obtained by silica gel chromatography [CH_2Cl_2/ MeOH (v/v, 10:1)]. Yield: 52% (50 mg). M.p.: 169–171 °C. ^{1}H NMR (300 MHz, $CDCl_3$): δ 8.21 (s, 1 H), 7.59-7.62 (m, 3 H), 7.54 (s, 1 H), 7.44–7.46 (m, 5 H), 7.24–7.34 (d, 4 H), 7.13–7.15 (m, 5 H), 6.54 (m, J = 6.9 Hz, 4H), 3.95 (q, 8H), 1.72–1.82 (m, 8H), 1.25–1.47 (m, 24H), 0.86 (m, 12H). ^{13}C NMR (900 MHz, DMSO-d_6): δ 159.2, 156.4, 145.1, 143.4, 141.1, 137.8, 137.3, 136.4, 135.6, 132.9, 130.4, 130.1, 127.1, 126.9, 124.6, 123.1, 122.1, 121.7, 105.8, 100.1, 91.8, 70.2, 68.8, 67.8, 67.4, 66.1, 31.0, 30.5, 28.6, 28.5, 25.2, 22.0, 13.8. UV/Vis (THF, nm): λ_{max} (ε) 345.5 (25 066), 474.5 (29 125). PL (THF, nm): λ_{max} 646. MS (MALDI-TOF) *m/z* calculated for $C_{70}H_{76}N_2O_6S_4$: 1168.4586; found, 1168.1948.

3-[5-(6-[Bis(2',4'-dihexyloxybiphenyl-4-yl)amino]thieno[3,2-*b*][1]benzothiophen-2-yl) thieno[3,2-b]thiophene-2-yl]-2-cyanoacrylic acid (SGT-125)

Compound **4c** (0.07 g, 0.037 mmol), dissolved in $CHCl_3$ (9 mL) and acetonitrile (9 mL), was condensed with 2-cyanoacetic acid (0.05 g, 0.65 mmol) in the presence of piperidine (0.02 g, 0.32mmol). The mixture was refluxed for 12 h. After cooling the solution, the organic layer was removed in vacuo. The red solid of **SGT-125** was obtained by silica gel chromatography [CH_2Cl_2/ MeOH (v/v, 10:1)]. Yield: 85% (63 mg). M.p.: 170–172°C. ^{1}H NMR (300 MHz, $CDCl_3$): δ 8.33 (s, 1 H), 7.95 (s, 1 H), 7.68 (d, J = 8.7 Hz, 1 H), 7.56 (d, 1 H), 7.42–7.51 (m, 4 H), 7.28–7.33 (m, 4 H), 7.15–7.18 (d, 5 H), 6.55 (m, J = 6.0 Hz, 4H), 3.99 (q, 8H), 1.73–1.82 (m, 8H), 1.25–1.48 (m, 24H), 0.86 (m, 12H). ^{13}C NMR (900 MHz, DMSO-d_6): δ 159.2, 156.5, 145.1, 145.0, 143.5, 142.9, 142.0, 141.9, 141.2, 139.6, 137.9, 137.3, 133.1, 130.4,

130.1, 126.7, 123.2, 121.7, 118.3, 117.0, 105.9, 100.1, 91.4, 68.8, 67.8, 31.0, 28.6, 28.5, 25.2, 22.0, 13.9. UV-vis (THF, nm): λ_{max} (ε) 345 (26 918), 467 (28 898). PL (THF, nm): λ_{max} 621. MS (MALDI-TOF) *m/z* calculated for $C_{68}H_{74}N_2O_6S$: 1142.4430; found, 1142.1804.

3-(6-[Bis(2',4'-dihexyloxybiphenyl-4-yl)amino]thieno[3,2-*b*][1]benzothiophene-2-yl)-2-cyanoacrylic acid (SGT-127)

Compound **5** (0.05 g, 0.05 mmol), dissolved in $CHCl_3$ (6 mL) and acetonitrile (6 mL), was condensed with 2-cyanoacetic acid (0.046 g, 0.54 mmol) in the presence of piperidine (0.023 g, 0.27mmol). The mixture was refluxed for 12 h. After cooling the solution, the organic layer was removed in vacuo. The orange solid of **SGT-127** was obtained by silica gel chromatography [CH_2Cl_2/ MeOH (v/v, 10:1)]. Yield: 64% (42 mg). M.p.: 161–163°C. ^{1}H NMR (300 MHz, $CDCl_3$): δ 8.36 (s, 1 H), 7.93 (s, 1 H), 7.77 (d, J = 6.9 Hz, 1 H), 7.44–7.52 (m, 6 H), 7.17–7.29 (m, 6 H), 6.54 (m, 4H), 3.97 (q, 8H), 1.73–1.86 (m, 8H), 1.25–1.50 (m, 24H), 0.87 (m, 12H). ^{13}C NMR (900 MHz, DMSO-d_6): δ 159.2, 156.50, 156.0, 154.8, 144.9, 141.9, 137.3, 132.8, 130.2, 127.4, 123.7, 123.5, 123.0, 121.7, 105.9, 101.5, 100.1, 99.9, 68.8, 67.8, 67.4, 30.9, 28.6, 25.2, 22.0, 13.9. UV/Vis (THF, nm): λ_{max} (ε) 344 (31 185), 459 (23 474). PL (THF, nm): λ_{max} 588. MS (MALDI-TOF) *m/z* calculated for $C_{62}H_{72}N_2O_6S_2$: 1004.4832; found, 1004.2767.

Chemical Characterization

The ^{1}H NMR spectroscopy study was conducted on a Varian Mercury 300 spectrometer using tetramethylsilane (TMS; d = 0 ppm) as the internal standard. Chemical shifts for the ^{1}H NMR spectra were recorded on a Varian Mercury 300 spectrometer using tetramethylsilane (TMS; d = 0 ppm) as the internal standard. The ^{13}C NMR spectroscopy study was conducted on a Bruker Biospin Gmbh AVAVCE II 900 spectrometer using tetramethylsilane (TMS; d = 0 ppm) as the internal standard. Chemical shifts for the ^{13}C NMR spectra were recorded on a Bruker Biospin Gmbh AVAVCE II 900 spectrometer using tetramethylsilane (TMS; d = 0 ppm) as the internal standard. MALDI-TOF mass spectra were recorded by a Voyager-DETM

STR biospectrometry workstation.

Instrumentations

UV/Vis absorption spectra were obtained in THF on a Shimadzu UV-2401PC spectrophotometer. Photoluminescence spectra were analysed with a Fluorolog FL-3-22 fluorimeter from Horiba–Jobin–Yvon Ltd., which was equipped with a 450 W Xe lamp and two analysing monochromators. Visible emission spectra were recorded with a Hamamatsu R928 photomultiplier. Cyclic voltammetry was performed on a Versa STAT3 (AMETEK) instrument. A three-electrode system was used and consisted of a reference electrode (Ag/AgCl), a working electrode (dye-coated TiO_2 films) and a counter electrode (Pt wire). The redox potentials of the dyes on TiO_2 were measured in CH_3CN with 0.1 m $TBAPF_6$ at a scan rate of 50 mV s^{-1}. Electrochemical impedance spectra of the DSSCs were measured with an impedance analyser (VersaSTAT3, AMETEK) connected to a potentiostat under dark conditions at room temperature. The spectra were scanned in a frequency range of 0.1–10^5 Hz with an amplitude of 10 mV at room temperature. Intensity-modulated photovoltage spectroscopy (IMVS) and intensity-modulated photocurrent spectroscopy (IMPS) were performed on an IviumStat (Ivium Technologies, Netherlands) supplied modulated light. IMVS and IMPS were measured under the illumination of an LED light source (λ = 635 nm) with different light intensities. The frequency range was 0.5–500 Hz.

Theoretical Calculations

All the theoretical calculations were performed with the Gaussian 09 program package on a computer workstation. The ground-state geometries were fully optimised without symmetry

constraints with Becke's three-parameter hybrid functional and Lee, Yang, and Parr's correlational functional (B3LYP) using the6-31G(d,p) basis set on all atoms. The electron-density-difference diagram and theoretical absorption spectra were calculated by TD-DFT at the same levels of theory in vacuum.

Time-Resolved Photoluminescence

Steady-state emission spectra of the dye sensitizers were measured with a FluoroLog-322 (Horiba) spectrometer equipped with a 450 W Xe arc lamp. Time-resolved photoluminescence (TR-PL) was measured using a time-correlated single-photon counting spectrometer (FluoTime 200, PicoQuant) equipped with a picosecond diode laser (LDH-P-C-390, PicoQuant) and a hybrid photomultiplier detector (PMA Hybrid 50, PicoQuant). The film samples consisting of dyes adsorbed on a layer of TiO_2 (3.5 μm thickness) or Al_2O_3 (4.0 μm thickness) were excited by laser pulse of approximately 100 ps at a centre wavelength of 393 nm, and the emission was measured at the $\lambda_{em\ max}$ of each dye. The time resolution of the TR-PL measurement was approximately190 ps, whereas it was effectively reduced to < 50 ps by deconvolution of the instrument response function.

Transient Photovoltage and Photocurrent Decay Measurements

In transient photovoltage measurements, the DSSCs were irradiated by a diode LED (635 nm) and the decay of the open-circuit voltage, caused by a stepwise decrease in a small fraction of the laser intensity, was measured. The resulting photovoltage decay transients were collected and the τ values are determined by fitting the data to the equation $\exp(-t/\tau)$.

DSSC Fabrication

A transparent nanocrystalline layer on the FTO glass plate was prepared by repeated screen printing with the TiO_2 paste (Dyesol, 18NR-T) and then dried at 120°C. The TiO_2 electrodes were gradually heated under flowing air at 325°C for 5 min, at 375°C for 5 min, at 450°C for 15 min, and at 500°C for 15 min. A paste for the scattering layer containing 400 nm anatase particles (CCIC, PST-400C) was deposited through screen printing and then dried for 1 h at 25°C. The TiO_2 electrodes were gradually heated under flowing air at 325°C for 5 min, at 375°C for 5 min, at 450°C for 15 min and at 500°C for 15 min. The resulting layer was composed of a 5.5 μm-thick transparent layer and a 3.5 mm-thick scattering layer. The thickness of the transparent layer was measured using an Alpha-step 250 surface profilometer (Tencor Instruments, San Jose, CA). The TiO_2 electrodes were again treated with $TiCl_4$ at 70°C for 30 min, and then sintered at 500°C for 30 min. The TiO_2 electrodes were immersed in the dye solution (0.3 mM in THF/EtOH=1:2 containing 20 mM CDCA) and kept at room temperature for 2 h. The counter electrodes were prepared by coating an FTO plate with a drop of H_2PtCl_6 solution (2 mg of Pt in 1 mL of ethanol) and it heating at 400°C for 15 min. The dye adsorbed on the TiO_2 electrode and the Pt counter electrode were assembled into a sealed sandwich-type cell by heating at 80°C with a hot-melt film (25 μm thick Surlyn) as a spacer between the electrodes. A drop of the electrolyte solution was placed on a drilled hole in the counter electrode of the assembled cell and was driven into the cell through vacuum backfilling. Finally, the hole was sealed by additional Surlyn and a cover glass (0.1 mm thick).

Photoelectrochemical Measurements of DSSCs

Photoelectrochemical data were measured using a 1000 W xenon light source (Oriel, 91193) that was focused to give 1000 W/m^2 at the surface of the test cell, which is equivalent to one sun at AM 1.5G. The light intensity was adjusted with a Si solar cell that was double-checked with an NREL-calibrated Si solar cell (PV Measurement Inc.). The applied potentials and measured cell currents were measured using a Keithley model 2400 digital source meter. Under these conditions, the current–voltage characteristics of the cell were determined by externally biasing the cell and measuring the generated photocurrents. This process was fully automated using Wavemetrics software. A similar data acquisition system was used to control the incident photon-to-current conversion efficiency (IPCE) measurement. Under full computer control, light from a 300 W Xe lamp was focused through a high throughput monochromator onto the photovoltaic cell under test. The monochromator was incremented through the visible spectrum to generate the IPCE (λ) curve as expressed in this equation (IPCE (λ) = 1240 (J_{sc}/l$_{\varphi}$)), where λ is the wavelength, J_{sc} is the current at short circuit (mA cm^{-2}), φ is the incident radiative (W m^{-2}). The IPCE curve can be derived from the measured absorption spectrum of the DSSC for comparison.

Acknowledgements

This work was supported by the National Research Foundation of Korea (NRF) grant funded by the Korea government (MSIP) (No. 2014R1A2A1A10051630 and No. 2014R1A1A1002511).

Notes and References

1 B. O'Regan and M. Grätzel, *Nature*, 1991, **353**, 737.

2 A. Hagfeldt, G. Boschloo, L. Sun, L. Kloo and H. Pettersson, *Chem. Rev.*, 2010, **110**, 6595.

3 S. Zhang, X. Yang, Y. Numata and L. Han, *Energy Environ. Sci.*, 2013, **6**, 1443.

4 M. Liang and J. Chen, *Chem. Soc. Rev.*, 2013, **42**, 3453.

5 (a) M. K. Nazeeruddin, A. Kay, I. Rodicio, R. Humphry-Baker, E. Mueller, P. Liska, N. Vlachopoulos and M. Grätzel, *J. Am. Chem. Soc.*, 1993, **115**, 6382; (b) C. Yasuo, I. Ashraful, W. Yuki, K. Ryoichi, K. Naoki and H. Liyuan, *Jpn. J. Appl. Phys.*, 2006, **45**, L638.

6 S. Mathew, A. Yella, P. Gao, R. Humphry-Baker, F. E. CurchodBasile, N. Ashari-Astani, I. Tavernelli, U. Rothlisberger, K. NazeeruddinMd and M. Grätzel, *Nat. Chem.*, 2014, **6**, 242.

7 (a) S. H. Kang, I. T. Choi, M. S. Kang, Y. K. Eom, M. J. Ju, J. Y. Hong, H. S. Kang and H. K. Kim, *J. Mater. Chem. A*, 2013, **1**, 3977; (b) M. S. Kang, S. H. Kang, S. G. Kim, I. T. Choi, J. H. Ryu, M. J. Ju, D. Cho, J. Y. Lee and H. K. Kim, *Chem. Commun.*, 2012, **48**, 9349.

8 A. Yella, R. Humphry-Baker, B. F. E. Curchod, N. Ashari Astani, J. Teuscher, L. E. Polander, S. Mathew, J.-E. Moser, I. Tavernelli, U. Rothlisberger, M. Grätzel, M. K. Nazeeruddin and J. Frey, *Chem. Mater.*, 2013, **25**, 2733.

9 L. E. Polander, A. Yella, J. Teuscher, R. Humphry-Baker, B. F. E. Curchod, N. Ashari Astani, P. Gao, J.-E. Moser, I. Tavernelli, U. Rothlisberger, M. Grätzel, M. K. Nazeeruddin and J. Frey, *Chem. Mater.*, 2013, **25**, 2642.

10 N. S. Baek, J.-H. Yum, X. Zhang, H. K. Kim, M. K. Nazeeruddin and M. Gratzel, *Energy Environ. Sci.*, 2009, **2**, 1082.

11 (a) H. N. Tsao, J. Burschka, C. Yi, F. Kessler, M. K. Nazeeruddin and M. Grätzel, *Energy Environ. Sci.*, 2011, **4**, 4921; (b) M. Zhang, Y. Wang, M. Xu, W. Ma, R. Li and P. Wang, *Energy Environ. Sci.*, 2013, **6**, 2944; (c) J. Yang, P. Ganesan, J. Teuscher, T. Moehl, Y. J. Kim, C. Yi, P. Comte, K. Pei, T. W. Holcombe, M. K. Nazeeruddin, J. Hua, S. M. Zakeeruddin, H. Tian and M. Grätzel, *J. Am. Chem. Soc.*, 2014, **136**, 5722.

12 Y.-S. Yen, H.-H. Chou, Y.-C. Chen, C.-Y. Hsu and J. T. Lin, *J. Mater. Chem.*, 2012, **22**, 8734.

13 S. Ahmad, E. Guillen, L. Kavan, M. Grätzel and M. K. Nazeeruddin, *Energy Environ. Sci.*, 2013, **6**, 3439.

14 M. Xu, M. Zhang, M. Pastore, R. Li, F. De Angelis and P. Wang, *Chem. Sci.*, 2012, **3**, 976.

15 G. Zhang, Y. Bai, R. Li, D. Shi, S. Wenger, S. M. Zakeeruddin, M. Grätzel and P. Wang, *Energy Environ. Sci.*, 2009, **2**, 92.

16 H. Qin, S. Wenger, M. Xu, F. Gao, X. Jing, P. Wang, S. M. Zakeeruddin and M. Grätzel, *J. Am. Chem. Soc.*, 2008, **130**, 9202.

17 W. Zeng, Y. Cao, Y. Bai, Y. Wang, Y. Shi, M. Zhang, F. Wang, C. Pan and P. Wang, *Chem. Mater.*, 2010, **22**, 1915.

18 R. Li, J. Liu, N. Cai, M. Zhang and P. Wang, *J. Phys. Chem. B*, 2010, **114**, 4461.

19 H. N. Tsao , C. Yi , T. Moehl, J.-H. Yum, S. M. Zakeeruddin, M. K. Nazeeruddin and M. Grätzel, *ChemSusChem*, 2011, **4**, 591.

20 (a) Z. Wang, H. Wang, M. Liang, Y. Tan, F. Cheng, Z. Sun and S. Xue, *ACS Appl. Mater. Interfaces*, 2014, **6**, 5768. (b) Z.-S. Huang, H.-L. Feng, X.-F. Zang, Z. Iqbal, H. Zeng, D.-B. Kuang, L. Wang, H. Meier and D. Cao, *J. Mater. Chem. A*, 2014, **2**, 15365. (c) H. Zhang, J. Fan, Z. Iqbal, D.-B. Kuang, L. Wang, H. Meier and D. Cao, *Org. Electron.*, 2013, **14**, 2071.

21 X. Hao, M. Liang, X. Cheng, X. Pian, Z. Sun and S. Xue, *Org. Lett.*, 2011, **13**, 5424.

22 P. Gao, H. N. Tsao, M. Grätzel and M. K. Nazeeruddin, *Org. Lett.*, 2012, **14**, 4330.

23 M. Zhang, J. Zhang, Y. Fan, L. Yang, Y. Wang, R. Li and P. Wang, *Energy Environ. Sci.*, 2013, **6**, 2939.

24 Y. Bai, J. Zhang, D. Zhou, Y. Wang, M. Zhang and P. Wang, *J. Am. Chem. Soc.*, 2011, **133**, 11442.

25 Q. Chai, W. Li, Y. Wu, K. Pei, J. Liu, Z. Geng, H. Tian and W. Zhu, *ACS Appl. Mater. Interfaces*, 2014, **6**, 14621.

26 D. P. Hagberg, J.-H. Yum, H. Lee, F. De Angelis, T. Marinado, K. M. Karlsson, R. Humphry-Baker, L. Sun, A. Hagfeldt, M. Grätzel and M. K. Nazeeruddin, *J. Am. Chem. Soc.*, 2008, **130**, 6259-6266.

27 Y. K. Eom, I. T. Choi, S. H. Kang, J. Lee, J. Kim, M. J. Ju and H. K. Kim, *Adv. Energy Mater.*, 2015, **5**, 1500300.

28 B. Košata, J. Svoboda, V. Novotná and M. Glogarová, *Liq. Cryst.*, 2004, **31**, 1367.

29 H. Chen, Q. Cui, G. Yu, Y. Guo, J. Huang, M. Zhu, X. Guo and Y. Liu, *J. Phys. Chem. C*, 2011, **115**, 23984.

30 C. Lô, A. Adenier, F. Maurel, J. J. Aaron, V. Kozmik and J. Svoboda, *Synt. Met.*, 2008, **158**, 6.

31 (a) K. Hara, Z.-S. Wang, T. Sato, A. Furube, R. Katoh, H. Sugihara, Y. Dan-oh, C. Kasada, A. Shinpo and S. Suga, *J. Phys. Chem. B*, 2005, **109**, 15476; (b) K. R. Justin Thomas, Y.-C. Hsu, J. T. Lin, K.-M. Lee, K.-C. Ho, C.-H. Lai, Y.-M. Cheng and P.-T. Chou, *Chem. Mater.*, 2008, **20**, 1830; (c) G. Li, K.-J. Jiang, Y.-F. Li, S.-L. Li and L.-M. Yang, *J. Phys. Chem. C*, 2008, **112**, 11591; (d) M. K. R. Fischer, S. Wenger, M. Wang, A. Mishra, S. M. Zakeeruddin, M. Grätzel and P. Bäuerle, *Chem. Mater.s*, 2010, **22**, 1836; (e)

H. Li, Y. Wu, Z. Geng, J. Liu, D. Xu and W. Zhu, *J. Mater. Chem. A*, 2014, **2**, 14649; (f) A. Baheti, K. R. Justin Thomas, C.-P. Lee, C.-T. Li and K.-C. Ho, *J. Mater. Chem. A*, 2014, **2**, 5766.

32 L. T. Cheng, W. Tam, S. H. Stevenson, G. R. Meredith, G. Rikken and S. R. Marder, *J. Phys. Chem.*, 1991, **95**, 10631.

33 P. Gao, Y. J. Kim, J.-H. Yum, T. W. Holcombe, M. K. Nazeeruddin and M. Grätzel, *J. Mater. Chem. A*, 2013, **1**, 5535.

34 (a) D. P. Hagberg, T. Marinado, K. M. Karlsson, K. Nonomura, P. Qin, G. Boschloo, T. Brinck, A. Hagfeldt and L. Sun, *J. Org. Chem.*, 2007, **72**, 9550; (b) R. Katoh, A. Furube, S. Mori, M. Miyashita, K. Sunahara, N. Koumura and K. Hara, *Energy Environ. Sci.*, 2009, **2**, 542; (c) K. D. Seo, I. T. Choi, Y. G. Park, S. Kang, J. Y. Lee and H. K. Kim, *Dyes Pigm*, 2012, **94**, 469.

35 J.-H. Yum, D. P. Hagberg, S.-J. Moon, K. M. Karlsson, T. Marinado, L. Sun, A. Hagfeldt, M. K. Nazeeruddin and M. Grätzel, *Angew. Chem. Int. Ed.*, 2009, **48**, 1576.

36 Li, X. Lv, D. Shi, D. Zhou, Y. Cheng, G. Zhang and P. Wang, *J. Phys. Chem. C*, 2009, **113**, 7469.

37 M. Xu, R. Li, N. Pootrakulchote, D. Shi, J. Guo, Z. Yi, S. M. Zakeeruddin, M. Grätzel and P. Wang, *J. Phys. Chem. C*, 2008, **112**, 19770.

38 (a) J. Liu, R. Li, X. Si, D. Zhou, Y. Shi, Y. Wang, X. Jing and P. Wang, *Energy Environ. Sci.*, 2010, **3**, 1924; (b) D. H. Lee, M. J. Lee, H. M. Song, B. J. Song, K. D. Seo, M. Pastore, C. Anselmi, S. Fantacci, F. De Angelis, M. K. Nazeeruddin, M. Grätzel and H. K. Kim, *Dyes Pigm*, 2011, **91**, 192; (c) K. Pei, Y. Wu, A. Islam, S. Zhu, L. Han, Z. Geng and W. Zhu, *J. Phys. Chem. C*, 2014, **118**, 16552; (d) A. Venkateswararao, K. R. J. Thomas, C.-P. Lee, C.-T. Li and K.-C. Ho, *ACS Appl. Mater. Interfaces*, 2014, **6**, 2528.

39 F. Paul, J. Patt and J. F. Hartwig, *J. Am. Chem. Soc.*, 1994, **116**, 5969.

40 J. K. Stille, *Angew. Chem. Int. Ed.*, 1986, **25**, 508.

41 E. Knoevenagel, *Chem. Ber.*, 1896, **29**, 172.

42 (a) J.-H. Yum, E. Baranoff, F. Kessler, T. Moehl, S. Ahmad, T. Bessho, A. Marchioro, E. Ghadiri, J.-E. Moser, C. Yi, M. K. Nazeeruddin and M. Grätzel, *Nat. Commun.*, 2012, **3**, 631; (b) M. J. Ju, J. C. Kim, H.-J. Choi, I. T. Choi, S. G. Kim, K. Lim, J. Ko, J.-J. Lee, I.-Y. Jeon, J.-B. Baek and H. K. Kim, *ACS Nano*, 2013, **7**, 5243; (c) I.-Y. Jeon, H.-J. Choi, M. J. Ju, I. T. Choi, K. Lim, J. Ko, H. K. Kim, J. C. Kim, J.-J. Lee, D. Shin, S.-M. Jung, J.-M. Seo, M.-J. Kim, N. Park, L. Dai and J.-B. Baek, *Sci. Rep.*, 2013, **3**, 2260.

43 A. Hagfeldt and M. Grätzel, *Chem.Rev.*, 1995, **95**, 49.

44 M. J. Frisch, G. W. Trucks, H. B. Schlegel, G. E. Scuseria, M. A. Robb, J. R. Cheeseman, G. Scalmani, V. Barone, B. Mennucci, G. A. Petersson, H. Nakatsuji, M. Caricato, X. Li, H. P. Hratchian, A. F. Izmaylov, J. Bloino, G. Zheng, J. L. Sonnenberg, M. Hada, M. Ehara, K. Toyota, R. Fukuda, J. Hasegawa, M. Ishida, T. Nakajima, Y. Honda, O. Kitao, H. Nakai, T. Vreven, J. A. Montgomery Jr., J. E. Peralta, F. Ogliaro, M. J. Bearpark, J. Heyd, E. N. Brothers, K. N. Kudin, V. N. Staroverov, R. Kobayashi, J. Normand, K. Raghavachari, A. P. Rendell, J. C. Burant, S. S. Iyengar, J. Tomasi, M. Cossi, N. Rega, N. J. Millam, M. Klene, J. E. Knox, J. B. Cross, V. Bakken, C. Adamo, J. Jaramillo, R. Gomperts, R. E. Stratmann, O. Yazyev, A. J. Austin, R. Cammi, C. Pomelli, J. W. Ochterski, R. L. Martin, K. Morokuma, V. G. Zakrzewski, G. A. Voth, P. Salvador, J. J. Dannenberg, S. Dapprich, A. D. Daniels, Ö. Farkas, J. B. Foresman, J. V. Ortiz, J. Cioslowski and D. J. Fox, *Gaussian 09*, 2009.

45 (a) S. E. Koops, P. R. F. Barnes, B. C. O'Regan and J. R. Durrant, *J. Phys. Chem. C*, 2010, **114**, 8054; (b) D. Zhou, N. Cai, H. Long, M. Zhang, Y. Wang and P. Wang, *J. Phys. Chem. C*, 2011, **115**, 3163.

46 (a) G. Boschloo, L. Häggman and A. Hagfeldt, *J. Phys. Chem. B*, 2006, **110**, 13144-13150; (b) E. M. Barea, C. Zafer, B. Gultekin, B. Aydin, S. Koyuncu, S. Icli, F. F. Santiago and J. Bisquert, *J. Phys. Chem. C*, 2010, **114**, 19840.

47 (a) T. Marinado, K. Nonomura, J. Nissfolk, M. K. Karlsson, D. P. Hagberg, L. Sun, S. Mori and A. Hagfeldt, *Langmuir*, 2010, **26**, 2592; (b) B. C. O'Regan and J. R. Durrant, *Acc. Chem. Res.*, 2009, **42**, 1799.

48 L.-L. Li, Y.-C. Chang, H.-P. Wu and E. W.-G. Diau, *Int. Rev. Phys. Chem.*, 2012, **31**, 420.

49 J. Bisquert, *Phys. Chem. Chem. Phys.*, 2003, **5**, 5360.

50 Q. Wang, J.-E. Moser and M. Grätzel, *J. Phys. Chem. B*, 2005, **109**, 14945.

51 X. Zong, M. Liang, C. Fan, K. Tang, G. Li, Z. Sun and S. Xue, *J. Phys. Chem. C*, 2012, **116**, 11241.

52 Z. Zhang, S. M. Zakeeruddin, B. C. O'Regan, R. Humphry-Baker and M. Grätzel, *J. Phys. Chem. B*, 2005, **109**, 21818.

53 H. M. Song, K. D. Seo, M. S. Kang, I. T. Choi, S. K. Kim, Y. K. Eom, J. H. Ryu, M. J. Ju and H. K. Kim, *J. Mater. Chem.*, 2012, **22**, 3786.

54 (a) D. Kumar, K. R. Justin Thomas, C.-P. Lee and K.-C. Ho, *J. Org. Chem.*, 2014, **79**, 3159; (b) S. Cai, X. Hu, Z. Zhang, J. Su, X. Li, A. Islam, L. Han and H. Tian, *J. Mater. Chem. A*, 2013, **1**, 4763.

55 (a) M. J. Ju, I.-Y. Jeon, J. C. Kim, K. Lim, H.-J. Choi, S.-M. Jung, I. T. Choi, Y. K. Eom, Y. J. Kwon, J.

Ko, J.-J. Lee, H. K. Kim and J.-B. Baek, *Adv. Mater.*, 2014, **26**, 3055; (b) M. J. Ju, I.-Y. Jeon, K. Lim, J. C. Kim, H.-J. Choi, I. T. Choi, Y. K. Eom, Y. J. Kwon, J. Ko, J.-J. Lee, J.-B. Baek and H. K. Kim, *Energy Environ. Sci.*, 2014, **7**, 1044.

56 A. Zaban, M. Greenshtein and J. Bisquert, *ChemPhysChem*, 2003, **4**, 859.

57 H. Chen, H. Huang, X. Huang, J. N. Clifford, A. Forneli, E. Palomares, X. Zheng, L. Zheng, X. Wang, P. Shen, B. Zhao and S. Tan, *J. Phys. Chem. C*, 2010, **114**, 3280.

58 E. Wang, Q. Meng, C. Wang, L. Li, H. Li and W. Hu, *Synt. Met.*, 2009, **159**, 1298.